Master of Science Thesis
VT2017

Dosimetric verification of synthetic CT using Cone Beam CT in an MRI only workflow

Emilia Palmér

Supervision
Petra Ambolt and Emilia Persson

Department of Medical Radiation Physics,
Clinical Sciences, Lund
Lund University
www.msf.lu.se

Abstract

Background and purpose: The MRI only workflow aims to base the treatment planning solely on magnetic resonance imaging (MRI), hence excluding the traditional computed tomography (CT) scan. To do that synthetic computed tomography (sCT) data is generated, replacing the conventional CT data. The aim of this study was to investigate the possibility of using cone beam computed tomography (CBCT) images to verify the sCT data. This was done via investigation of the properties of the kV CBCT systems in the clinic and comparing dose distributions carried out on both the sCT and the CBCT data.

Materials and methods: Several phantom measurements were made on the kV CBCT systems on the six Varian TrueBeam™ linac used in the clinic. The properties investigated were the variation in Hounsfield Units (HUs) over time for one kV CBCT system as well as variation between the six kV CBCT systems. The HUs of one kV CBCT system was also compared to HUs from a Siemens CT system. Using 28 CBCT data sets from seven patients, a HU to relative electron density (RED) table was created. Treatment plans (RapidArc) were calculated on sCT, CT and CBCT images using the standard HU-RED table based on CT HU. For the CBCT data, additional calculation was done using the HU-RED table based on CBCT HU. The difference between the dose distributions was evaluated comparing clinical dose volume histograms (DVH) and mean absorbed doses.

Results: The phantom measurements showed that the kV CBCT system was stable in HU over time. All six kV CBCT systems generated comparable HU values. The variation of HUs between CT and CBCT images was minor. The CBCT images, however, exhibited larger variation across the field of view (FOV) compared to CT images. Dose calculation based on CBCT data showed a mean dose difference to PTV of 0.0% (HU-RED CT) and -0.8% (HU-RED CBCT) compared to dose calculations based on sCT data.

Conclusion: The HUs for one kV CBCT system were found to stable over time. The variation between the six kV CBCT systems were found to be minor. Results obtained for one system can therefore be transferred onto all the systems. The minor difference in HUs between CT and CBCT images indicates that a correction of HUs is not necessary to obtain sufficiently accurate absorbed dose calculations on CBCT images. The compared dose distributions based on CBCT and sCT data showed good agreement in terms of dose accuracy, regardless of which HU-RED table used. This indicates that CBCT data can be used to verify sCT data.

Popular scientific summary in Swedish

En tredjedel av de män som diagnostiseras med cancer i Sverige idag diagnostiseras med prostatacancer. Prostatacancer är den vanligaste förkommande cancerformen i Sverige. Det finns flera behandlingsmetoder för prostatacancer, en utav dem är extern strålbehandling. Vid behandling med denna metod bestrålas prostatan med en strålkälla som befinner sig utanför kroppen. En liten stråldos ges vid flera olika tillfällen och det är viktigt att man ligger likadant vid varje tillfälle.

Innan man kan starta sin strålbehandling måste vissa förberedelser utföras. Ett vanligt förberedande steg för prostatacancerpatienter är att genomgå en magnetresonans (MR)-undersökning. Detta är en undersökning som med hjälp av magnetism skapar tredimensionella bilder av kroppens inre. MR är en bildmetod som ger anatomisk information och har fördelen att mycket gott kunna avbilda mjukvävnad som till exempel prostatan. Bildmetoden har även goda förutsättningar att visa tumörutbredning. Detta ger att man noggrant kan bestämma cancerns utbredning och läge.

Patienterna genomgår även en datortomografi, kallad CT. Detta är en undersökning som med hjälp av röntgenstrålar skapar tredimensionella bilder av kroppens inre. Förutom att ge anatomisk information ger bilderna även information om hur röntgenstrålningen dämpas i kroppen. Med kombination av MR- och CT-bilder bestämmer läkare vilket område som ska bestrålas och vilka områden som ska undvikas för att skona känsliga organ. Sedan görs en behandlingsplan där man detaljerat planerar så att rätt mängd stråldos hamnar på rätt plats.

För att möjliggöra ett enklare arbetsflöde har forskare visat ett intresse för att enbart använda sig av MR-bilder i förberedelserna och utesluta CT-bilder. Detta gör att de osäkerheter som tillkommer då man kombinerar de båda bildtyperna försvinner. Dock har man problemet att MR-bilder inte ensam besitter den information som krävs för att skapa behandlingsplaner. För att lösa detta har man utvecklat en metod som omvandlar MR-bilderna till bilder som ser ut och kan användas inom dosplanering på samma sätt som CT-bilderna. Dessa bilder kallas syntetiska CT-bilder.

De olika stegen i förberedelserna inför strålbehandling kontrolleras av sjuksköterskor, läkare och fysiker för att säkerhetsställa att allt är korrekt. Vid införande av syntetiska CT-bilder behövs ett tillvägagångssätt för att kontrollera att de skapade bilderna är korrekta. Idag görs detta genom att jämföra de syntetiska CT-bilderna mot de fortfarande existerande CT-bilderna. Men om CT-bilderna ska tas bort krävs ett annat tillvägagångssätt. Detta arbete föreslår en metod för hur detta skulle kunna gå till samt utvärderar resultatet och jämför mot den redan existerande metoden. Den nya metoden utgörs av att de syntetiska CT-bilderna jämförs mot en bild som tas på patienten inne i behandlingsrummet med behandlingsapparaten. Resultatet av studien visar att den nya föreslagna metoden på ett lovande vis kan användas för kontroll av syntetiska CT-bilder. Med vidare undersökning kan den nya metoden införas i den kliniska verksamheten.

Acknowledgments

First of all, I would like to thank my supervisors:

Petra Ambolt, thank you for giving me the opportunity to work with this project. Your support and motivation have helped me throughout this thesis.

Emilia Persson, thank you for always being close at hand. Your endless help and guidance throughout this thesis has been invaluable.

A special thanks to Christian Gustafsson for your support and help in programming when my own knowledge in the field were lacking.

I would like to thank Spectronic Medical AB for generating the sCT used in this thesis. Without them, this project would not have been achievable.

A thank to Lars E Olsson and Lee Ambolt for structuring and correcting this thesis.

Thank you, Joakim Nilsson, for helping me with the treatment planning.

I would also like to thank Lars E Olsson, Sofie Ceberg, Elinore Wieslander and Lars Weber for your participation in brainstorming ideas.

Abbreviations

EBRT	External Beam Radiotherapy
CT	Computed Tomography
HU	Hounsfield Unit
TPS	Treatment Planning System
RED	Relative Electron Density
PTV	Planning Target Volume
OAR	Organ at Risk
MRI	Magnetic Resonance Imaging
sCT	Synthetic Computed Tomography
CBCT	Cone Beam Computed Tomography
MDCT	Multidetector row CT
2D	Two-dimensional
FPD	Flat-panel detector
3D	Three-dimensional
FOV	Field of View
SDA	Statistical Decomposition Algorithm
MeAE	Median Absolute Error
SD	Standard Deviation
ROI	Region of Interest
CTV	Clinical Target Volume
AAA	Anisotropic Analytical Algorithm
MICE	Medical Interactive Creative Environment

Table of contents

1. Introduction

1.1. Background

In 2014 cancer was the second most common cause of death in Sweden, and about 64 000 cases were registered [1]. A common approach to treat cancer is to use radiation therapy that uses radiation with high energy photons. Radiation therapy accounts for 30 percent of all cancer cures and about half of all cancer patients receive radiation therapy at some point during their treatment [2]. External beam radiotherapy (EBRT) is a non-invasive type of radiation treatment, with the aim of delivering high absorbed dose to the tumour while keeping the dose as low as possible to the surrounding normal tissue. In order to achieve that goal, a high accuracy is required in the treatment process.

There are different steps in the treatment process, which together can be described as a radiotherapy workflow. This starts with a treatment prescription and ends with a completed treatment. One step in the workflow is an examination with an imaging modality called computed tomography (CT). The CT image provides Hounsfield Units (HUs) that the treatment planning system (TPS) requires. To be able to perform absorbed dose calculations the TPS converts HU to corresponding relative electron density (RED). The RED is the electron density in a material relative to the electron density in water. The CT images are also used when delineating the planning target volume (PTV) and the organs at risk (OAR), which the TPS uses to develop an advanced treatment plan.

For some diagnoses, such as prostate cancer, magnetic resonance imaging (MRI) is preferred as a complementary imaging modality. The MRI images enables a more accurate definition of the prostate target volume and delineation of the OARs due to the superior soft tissue contrast of MRI images compared to CT images [3]. When both CT and MRI images are used, a co-registration of the two image data sets are used to create a treatment plan. The MRI enables accurate target delineation and the CT provides the HUs needed for absorbed dose calculation. Although this is a common procedure, the co-registration process is associated with systematic registration uncertainties. It has been estimated that the registration error for prostate plans is approximately 2 mm for an automated registration process. The registration error is based on average offset in the three orthogonal dimensions [4]. The reason for the uncertainty is variation in patient set up and the elapsed time between the two scanning modalities. The anatomical relationship for some organs may have changed while waiting for the second imaging, such as filling of the rectum and/or bladder [4]. Therefore, interest has been directed towards a workflow using MRI as the only imaging modality – often denoted as an MRI only workflow.

MRI only radiotherapy excludes the co-registration between CT and MRI images and hence the systematic registration errors will be reduced [4]. It will also simplify the workflow, and reduces the workload and therefore become more cost effective [5]. Another advantage of using MRI only is a tighter delineation of the mean prostate volume, a result of the improved image contrast. The delineation in the MRI has been shown to be smaller (32-40%) than delineated in the CT. This leads to a more precise description of the prostate target volume, and the possibility of sparing more surrounding tissue and OARs from irradiation [3][6][7]. Although, one should consider that the outcome of treatment when using a tighter delineation of the prostate volume has not been investigated. The Swedish consortium Gentle Radiotherapy (www.gentleradiotherapy.com) has since 2013 been working towards a radiotherapy workflow incorporating all advantages of using MRI in radiotherapy. The project is currently in the process of implementing the MRI only workflow for a number of different diagnoses.

An obstacle using an MRI only workflow is the absence of HUs in the MRI which are required for absorbed dose calculation. A solution to solve this is to introduce a conversion step to replace the co-registration step. The conversion step consists of creating a synthetic CT (sCT) data set from the MRI image. The sCT images is a substitute for the CT images and is generated via various methods [8]–[16]. One way to verify if the HUs in the sCT images are generated correctly is to compare

absorbed dose calculations done on the sCT data and the CT data. But in an MRI only workflow the CT is not a part of the imaging procedure, and hence another method for sCT data verification must be considered. An previous suggested idea to verify the sCT data is to use a cone beam CT (CBCT) data set [17]. The CBCT is a kilovoltage based imaging modality used to confirm the patient set up in the treatment room before treatment.

1.2. Aim

The aim of this study was to evaluate a method to verify the sCT image when there is no CT image available, using the CBCT image instead. This includes two parts; investigating properties of the kV CBCT systems with phantom measurements, and developing a HU to RED table based on CBCT images. To evaluate the table, a treatment plan is created and applied on both the sCT and CBCT images. Absorbed dose calculations are carried out on each data set and the two dose distributions are compared.

2. Theory

2.1. Imaging modalities

2.1.1. Computed Tomography

The CT was first introduced to the world and clinic in 1971 and was used for diagnostics. The image consists of measured x-ray transmission profiles that have passed thorough the patient in many angles. To accomplish a profile a detector arc is required. This generally consists of 800-900 elements lined up in a row. The x-ray tube and the detector package is mechanically interconnected and rotates around the patient. Using a number of detector rows aligned provides a more rapid acquisition. This is called a multidetector row CT (MDCT) and this method shortens the scan time, permits larger scan areas and enables thinner slices [18].

The imaging system setup for a CT is an x-ray tube, collimators, beam shaping filters and detector. These components can be found in the gantry and are rotated around a sliding table, creating a helical CT [18].

The beam from the x-ray tube is collimated into a fan shape. Filters are positioned directly after the output from the x-ray tube. These filters are called the flattening filter and bow-tie filter. Flattening filters remove low energy x-rays from the beam, sparing the patient from unnecessary extra dose. Bow-tie filers shape the energy distribution across the beam according to the shape of the patient. After exiting the patient, the beam is collimated by a grid which rejects the scattered photons [18].

The CT detectors are scintillators and photodiodes. The detector row is divided into detector elements separated by septa to prevent light from one element being detected in a neighbouring element. In a MDCT the detector arc consists of up to 320 detector rows making it possible to cover up to 16 cm longitudinally in a single rotation [18].

The measured transmission profiles are used to reconstruct the CT image. This is done via an analytic method or an iterative method resulting in a matrix of pixels. Each pixel has a value that corresponds to the linear attenuation coefficient of the tissue present along the relevant transmission path. The linear attenuation coefficient depends on the density and composition of the material and the photon energy. The matrix of linear attenuation coefficients is then transformed into a corresponding matrix of Hounsfield Units (HU). HU is described in more detail in 2.2. This is a scale of radiodensity that is expressed relative to the linear attenuation coefficient of water at room temperature [18].

2.1.2. Cone Beam Computed Tomography

A CBCT is a CT scanner developed to cover large scanning areas in one rotation. This makes it suitable for different clinical applications such as pre-treatment verification of patient positioning and target volume localization in radiotherapy. The CBCT has different design features, image quality characteristics and application domains compared to the MDCT scanner. The largest difference is that the CBCT uses a two-dimensional (2D) digital flat-panel detector (FPD) to yield a three-dimensional (3D) volumetric image in just one rotation. One can consider that the 2D detector array has replaced the rows of detector elements [19].

In a CBCT the x-ray tube generates a broad, cone-shaped beam of radiation. To do that the x-ray tube is designed with a larger anode angle compared to the MDCT x-ray tube. This results in a field of view (FOV), in one rotation, to be as large as 25 cm in the rotating direction and 20 cm in the z-direction. The down side to using a large FOV is that the entire volume generates scatter radiation contributing to a significantly poorer image quality [19].

The filtration in a CBCT involves a bow-tie filter. It contributes to lower absorbed dose to the patient and improves tomographic imaging quality since it improves the uniformity, HUs accuracy and contrast-to-noise ratio. The disadvantage to using a bow-tie filter is that the detector efficiency decreases due to beam hardening [19]. This phenomenon occurs since the x-ray source emits a broad spectrum of energies where photons of higher energies typically attenuates less. This leads that the mean energy of the emitted x-rays increases when passing an object, causing an underestimation of the objects thickness.

There are two different acquisition modes that can be used when imaging with a CBCT. These provide two different FOVs, full-fan mode and half-fan mode seen in Figure 1. When the image target is less than 24 cm in width the full-fan mode is appropriate. For larger objects, such as the pelvis, the half-fan mode is preferable [20]. Using the latter mode, the object is scanned asymmetrically using two 180° rotations at which the FPD is shifted laterally for the second rotation and a half bow-tie filter is used. This enables coverage of larger areas [19].

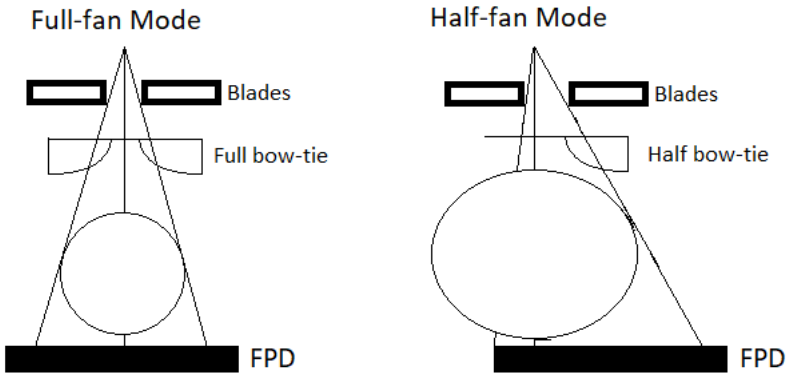

Figure 1. The acquisition modes for CBCT. To the left the full-fan mode is illustrated and to the right the half-fan mode. Image inspired from [20]

Using a FPD makes it possible to use a wide cone beam and thus a large longitudinal coverage and it enables high spatial resolution. The high spatial resolution makes the CBCT suitable for imaging high-contrast structures. The FPDs dynamic range of meeting the linearity condition between input signal and output signal is lower compared to the detector system in MDCT scanners, resulting in lower soft tissue contrast and longer scan time. The FPD can consist of a matrix of detector elements from 5 x 5 cm^2 to 40 x 40 cm^2. This makes it possible to image an entire organ such as brain, heart or liver in just one axial scan [19].

In radiation therapy, the CBCT is mainly used for patient positioning registering the CBCT image with the planning CT image. The target can be precisely aligned with the therapeutic x-ray beam from the linear accelerator. Most treatment centres use a kV CBCT where the x-ray tube and FPD is mounted on the gantry of the linear accelerator in an orientation that is orthogonal to the therapeutic beam. When imaging, the gantry rotates 360° creating a tomographic image. The CBCT image is sometimes also used during the radiotherapy treatment course for detection of day to day anatomical changes in soft tissue such as intestinal movement [19].

2.1.3. Synthetic Computed Tomography

In comparison to CT images, the MRI images does not provide physical properties of the tissue such as HUs. The HUs are converted into electron densities required for absorbed dose calculations. Over the past years, several different methods for converting MRI data into sCT

data have been suggested [8]–[16]. Most of them are in-house developed, but commercial solutions have also been presented [15][16].

There are different approaches for in-house developed sCT softwares. One method is to apply bulk electron densities to the MRI. The original pixel values are overwritten with a single electron density value. This could be applied on the entire body or on segmented contoured structure volumes [10][11]. Another method is the atlas-based method where MRI atlas and conjugate electron density atlas is used. The MRI atlas is based on manually delineated MRI images and is used to automatically segment organs. The conjugate electron density atlas is based on co-registered MRI and CT images. It is used to map electron densities to the segmented MRI image, creating a sCT image [8].

Skåne University Hospital and Norrland University Hospital has together with Spectronic Medical AB developed a method that automatically generates sCT directly from the MRI, using the Statistical Decomposition Algorithm (SDA) [16]. The method has since become a commercial solution, MriPlanner™ (Spectronic Medical AB, Helsingborg, Sweden) and is currently in use for external radiotherapy of prostate cancer within the study MR-only Prostate RadiOTherapy Excluding CT (MR-PROTECT). The SDA is a population driven algorithm that automatically generates sCT images from standard T2 weighted MRI images. Using a template database containing MRI and CT image pairs and automatic tissue segmentation, the algorithm estimates the most probable CT images representation for the incoming MRI images [16].

To decompose and delineate the tissue classes in the incoming MRI images, the SDA applies an automated segmentation algorithm. After that, each set in the template database is deformed so that their segmented structures align with the ones on the incoming MRI images. The result is then applied to the respective template CT data sets. From this, the most probable CT images representation of each tissue type is found in the template database. The found tissue types are then fused together into one final sCT data set [16].

Since the sCT images is derived from the MRI images, the sCT images has the same resolution, frame of reference, body outline and FOV as the MRI images. The main requirement for the incoming MRI images is that the acquisition of the contrast broadly resembles the template MRI images since the SDA mainly operates by identifying and structuring visual features in the image. The incoming MRI image also has additional requirements to allow dose calculation on the generated sCT image. The FOV must encompass the entire volume of the patient and since spatial resolution in the sCT images is equal to the resolution in the incoming MRI images it must be sufficient [16]. The MRI acquisition sequence parameters used in this thesis were the same as presented in the MR-Only Prostate External Radiotherapy (MR-OPERA) study [21].

Creating sCT images using SDA and comparing the average mean absorbed dose difference in PTV between sCT images and registered CT images, the difference was 0.0% $\pm$ 0.2% (1 SD). Compared to the uncertainties with the uncertainties that may arise from varying patient positioning between imaging sessions, the dosimetric uncertainties coupled to the SDA are notably lower and clinically negligible [16].

In the MR-OPERA study, the ability to verify dosimetric accuracy and robustness in the commercially available software MriPlanner™ was investigated. This software converts the MRI images to sCT images of the male pelvis using SDA. The dose differences between plans generated on CT images and sCT images was small. The result was statistically equivalent at a 95% confidence level within $\pm$0.5%. Catastrophic errors were not found in the sCT image conversion in the MR-OPERA study. Although, an outlier detection is needed when introducing

an MRI only workflow. The outlier detection should detect errors in the sCT image and prevent the treatment planning process to continue. The authors suggested that a sanity check of the HU distribution in the CT images and sCT images could be done and that it would be sufficient [21] However, since the aim for an MRI only workflow is to exclude the CT images entirely another method for outlier detection must be developed. One suggestion could be to use the CBCT images to verify the sCT images.

2.2. Hounsfield Units

HU are a transformation of the linear attenuation coefficient of the interacting material ($\mu_{material}$) and are expressed relative to the linear attenuation coefficient of water at room temperature (μ_{water}). The corresponding HU of a voxel is given by equation 1.

$$HU_{material} = \frac{\mu_{material} - \mu_{water}}{\mu_{water} - \mu_{air}} \cdot 1000 \quad (1)$$

meaning that a change of 1 HU corresponds to a change of 0.1% of the linear attenuation coefficient of water. Water has a HU of zero since $\mu_{material} = \mu_{water}$ and air a HU of -1000 since $\mu_{water} = 0$ [18]. Typical HUs for different tissues, measured in a CT image, can be studied in Table 1.

The output from the x-ray tube consists of a range of photon energies resulting in a non-constant μ. The photon energy selected will therefore generate different HU in the same object. Due to differences in average photon energy in the x-ray spectra, the materials exhibit a non-linear relationship to their linear attenuation coefficient relative to water. The μ for water increases at lower energies, resulting in beam hardening. The reconstructing algorithm for CT applies a correction for beam hardening in water forcing the μ to be constant for water. Other materials will have a μ depending on density and structure of the material and the beam hardening [22].

Calibrations of the HU and beam hardening corrections is done for the MDCT. This is typically absent for the CBCT and the values for HUs are more variable compared to those from the MDCT. The uniformity of the HU in an entire cross-section of a homogenous object is not uniform. At the edges the HUs decrease [19]. When scanning bigger objects such as the pelvis and doing larger volumetric reconstructions the effect of scatter becomes substantial. X-ray scatter results in artifacts in the image such as cupping artifacts and/or streak artifacts and quantitative inaccuracy in reconstructed HU [23].

Table 1. Typical HU values for different types of tissues measured in a CT image. The range is from about -1000 HU to 1000 HU. The higher density a material has, the higher the HU becomes. The values are taken from Dance et al. [18]

Tissue	**HU**
Compact bone	+1000 (+300 to + 2500)
Liver	+60 (+50 to +70)
Muscle	+25 (+10 to +40)
Water	0
Fat	-90 (-100 to -80)
Lung	-750 (-950 to -600)
Air	-1000

2.3. Dose calculation on CBCT

Richter *et al.* [24] investigated the feasibility and accuracy for dose calculation in CBCT images acquired from the CBCT system Synergy XVI Elekta. This was done to establish if CBCT images could be used for treatment planning. Phantom measurements were performed to investigate the relationship between HU and corresponding RED for different materials in both planning CT and CBCT images. From these measurements, density calibration tables (HU-RED table) were specified. These were the standard HU-RED CT table and the phantom based HU-RED CBCT table. Dose calculation on the phantom CBCT image was performed with the standard HU-RED CT table and the phantom based HU-RED CBCT table. The dose distributions were compared with the dose distribution carried out on planning CT images. The comparison showed that calibration using phantom based HU-RED CBCT table gave least deviation between the dose distributions calculated on CT and CBCT images. Dose calculations on patient CBCT images were performed using either the standard HU-RED CT table, the phantom based HU-RED CBCT table, the patient group based HU-RED CBCT table or the patient individual HU-RED CBCT table. A patient group based HU-RED CBCT table was developed using many patients CBCT images, calculating mean HU values for tissues. A patient individual HU-RED CBCT table was determined for each patient, resulting in every patient having an individual table. Using the standard HU-RED CT table and the phantom based HU-RED CBCT table led to inaccurate dose distribution on CBCT images in pelvis patients. The patient group and patient individual based HU-RED CBCT tables generated accurate dose distribution in the pelvis region. The final result indicated that accurate dose distribution could be feasible in CBCT images if correction of the HUs were done.

de Smet *et al.* [25] studied the accuracy of dose calculation on kV CBCT images of lung cancer patients. First, they investigated the variation in CBCT HU for six Varian On-Board Imager TrueBeam system using a phantom. The result showed good correspondence between the systems. The maximum difference was 30 HU for Teflon. Further, they looked up the difference in HU between CBCT and CT images for lung patients. They concluded that HUs for lung tissue varied too much to rely on manually overriding densities and then perform dose calculations. The Varian On-Board Imager TrueBeam had small difference between CT and CBCT HU numbers for high density tissues in the thorax region, for example muscle. Therefore, a patient group HU-RED CBCT table was produced correcting only for the average differences in HU for lung tissue of six lung patients. Dose calculation using the standard HU-RED CT table was performed on CBCT images. The dose distribution was then recalculated using the patient group or patient specific HU-RED CBCT table. The patient group and the patient specific HU-RED CBCT table for Varian On-Board

Imager TrueBeam gave approximately the same result when calculating dose distributions. The result showed 1%-2% difference in dose distribution compared to the distribution calculated on CT images. The standard HU-RED CT table gave results with differences of 2%-3%. The overall result indicated that accurate dose distribution could be obtained on CBCT images without HU correction for the Varian On-Board Imager TrueBeam system.

Dunlop *et al.* [26] performed an investigation comparing different CT number calibration techniques for CBCT based dose calculation. The CBCT system used in this study was XVI (v.4.5) Elekta. One technique was to use a CBCT reconstruction to adjust the HUs. The reconstruction was corrected for scatter using an in-house software. Then a patient-independent table was applied to the reconstructed images to convert HU in to RED. Another technique evaluated was density overrides. The "water only", "water-and-bone" and "water-and-lung" methods were investigated. For "water only" all tissue was assigned as water. For "water-and-bone" was the tissue assigned as either water or bone and for "water-and-lung" was the tissue assigned either as water or lung. Also investigated was the CBCT density-assignment tools available in the TPS where six different densities were assigned to the CBCT image. The study showed that HU adjustment using CBCT density-assignment tools provided a similar CBCT dose calculation as the calculation done on CT images. It was the best method for pelvis patients without excess adipose tissue and was the method they recommend for accurate dose calculations.

Edmund *et al.* [17] examined the possibility of using CBCT guided treatment delivery and planning verification for MRI only radiotherapy of the brain. The CBCT images in the study was acquired from Varian On-Board Imager (v.1.6). In MRI only radiotherapy one step was to estimate if the CBCT data could provide reliable error estimation of the sCT data. To do that they needed to transform the CBCT HU to RED using conversion curves. These were either phantom based or population based. To quantify the error estimation, they statistically evaluated the median value of the binned absolute errors. When transferring the data into RED the median absolute error (MeAE) value for CT data and CBCT data became closer. The conclusion was the correctness of sCT data could be verified from CBCT data using a population based conversion curve.

The conclusion for all studies was that treatment planning on CBCT images was feasible. Some of the studies estimated that a HU-RED table based on CBCT images, correcting the HUs, was required to obtain an accurate dose distributions.

3. Materials and methods

3.1. Phantom measurements

3.1.1. Phantom material

The phantom used was the CIRS Model 062M Electron Density Phantom with associated electron density plugs. The phantom consists of two nested disks made of Plastic Water®-LR. The inner disk represents a brain configuration. Combining the outer and inner disk represents an abdomen configuration. In this study, the abdomen configuration was used. Ten different tissue equivalent electron density plugs can be positioned in seventeen different locations within the phantom. The tissue types and corresponding RED can be seen in Table 2. Two additional 50 mm thick bolus slabs made of Plastic Water®-LR were used as scattering material as recommended in the user guide [27] by the manufacturer (Computerized Imaging Reference Systems, INC., Norfolk, Virginia, USA).

The images analysed and all the measurements in this study were acquired from the kV CBCT system used for image-guided radiotherapy, Varian On-Board Imager™ TrueBeam™.

Evaluations of the phantom measurements were carried out on the CBCT images in the registration module Eclipse Image Registration (Varian Medical Systems v. 13.6, Palo Alto, CA).

Table 2. Tissue and corresponding RED for the different phantom electron density plugs.

Tissue	**RED**
Lung Inhale	0.190
Lung Exhale	0.489
Adipose	0.949
Brest 50% Gland 50% Adipose	0.976
Water	0.998
Muscle	1.043
Liver	1.052
Solid Trabecular Bone 200 mg/cc HA	1.117
Solid Dense Bone 800 mg/cc HA	1.456
Solid Dense Bone 1250 mg/cc HA	1.695

3.1.2. Constancy of HU over time

To confirm that the measurements done on CBCT images can be used in the future, an investigation of constancy of HU over time was made. A weekly CBCT measurement was carried out on one out of six available Varian On-Board Imager™ TrueBeam™ in our clinic where MRI only treatments currently are scheduled. The CIRS phantom was the object imaged. This had the recommended arrangement seen in Figure 2, for optimal positioning of the electron density plugs according to the manufacturer (Computerized Imaging Reference Systems, INC., Norfolk, Virginia, USA). Figure 2 also displays the setup of the phantom.

The image was obtained in CBCT Pelvis Mode, that is in half-fan mode and a 360° rotation of the gantry. The parameters were 125 kV, 1080 mAs and the reconstruction was set to 3 mm slice thickness. The electron density plugs were evaluated in the CBCT images using the profile tool in Eclipse Image Registration. This can be seen in Figure 3.

The values noted for each individual profile were the minimum, maximum, mean and the standard deviation (SD). The aggregated mean value of the individual mean HU values was calculated as well as the associated SD.

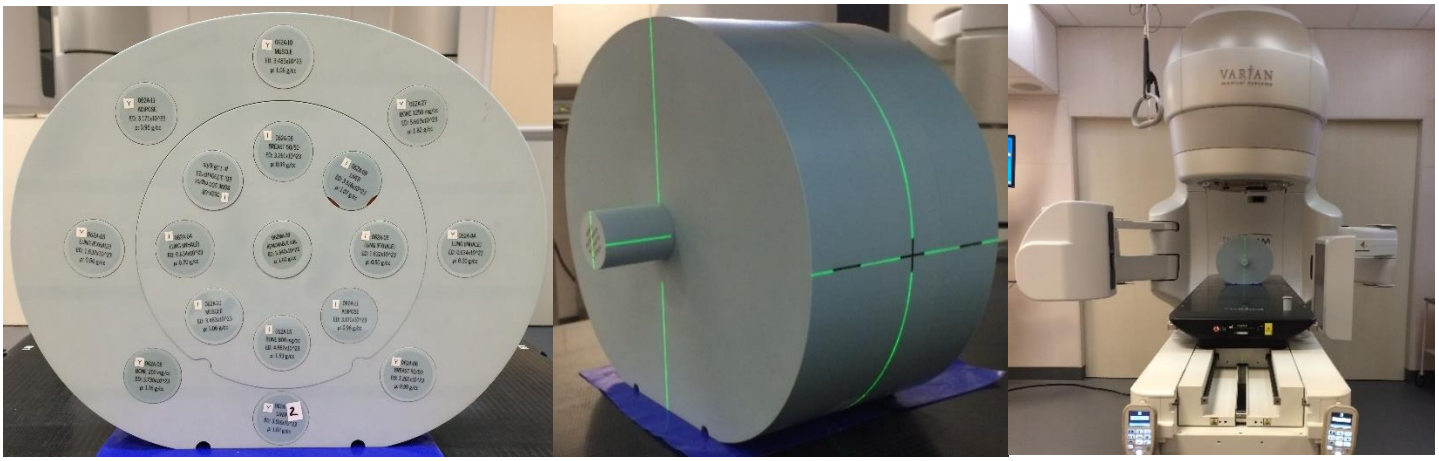

Figure 2. To the left, the recommended arrangement of the tissue electron density plugs is seen. In the middle and to the right, the setup of the phantom.

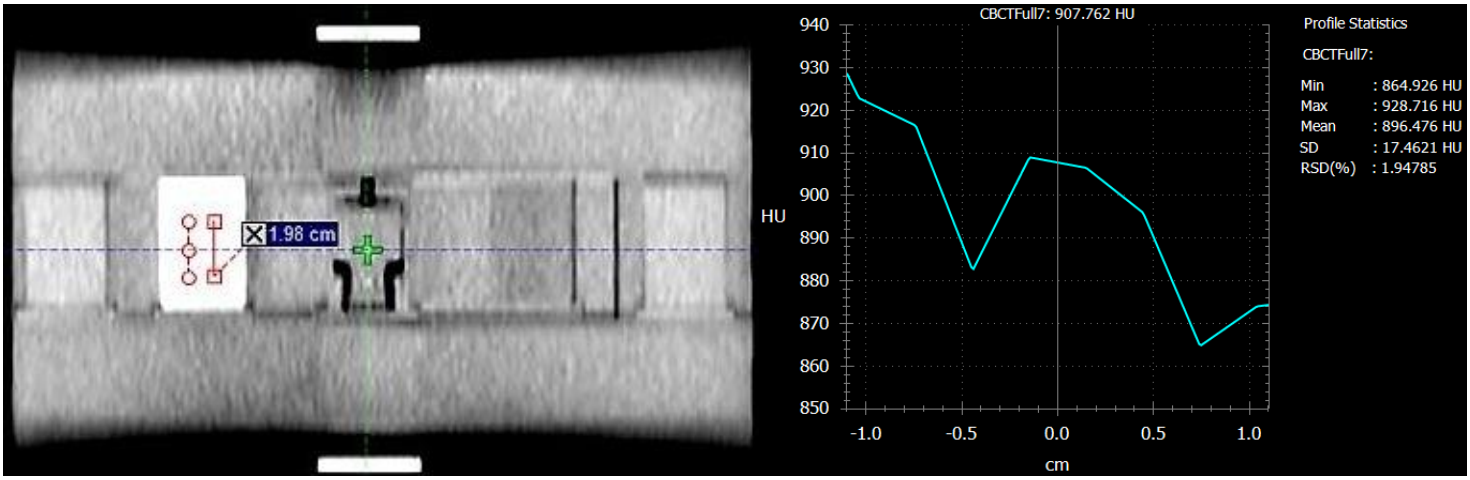

Figure 3. The profile used when extracting HU for each material. The profile was placed in the centre of each material. In this image, the profile is drawn in Bone 800 mg/cc HA.

3.1.3. Consistency of HU between kV CBCT systems

To investigate whether the HUs are constant between the kV CBCT systems in the clinic, an identical measurement was carried out on each of the six systems. The same setup and acquisition mode as the constancy over time measurements was used for each machine.

The images were evaluated in Eclipse Image Registration using a profile acquired from each material, as can be seen in Figure 3Figure 3. The mean and SD values were noted. For all the measurements, the aggregated mean value of the individual mean HU values was calculated along with the corresponding SD.

3.1.4. Constancy of HU in FOV

It was of interest to know if the signal in different parts of the FOV was constant for dissimilar materials. The materials used to evaluate the constancy were the electron density plugs equivalent to lung inhale, water and solid dense bone 1250 mg/cc. These are materials with low, medium and high RED. The same setup and acquisition mode was used as for the constancy over time measurements. Five measurements were carried out for each material with the respective plug positioned in different cavities for each measurement. Position were the centre,

left, right, upper and lower cavity of the phantom. The surrounding cavities were filled with water equivalent material.

An image was obtained for each position of the materials and the mean HU value was evaluated in Eclipse Image Registration using a region of interest (ROI) within an area of 1 x 1 cm applied as centred as possible in the plug. An example is shown in Figure 4 with solid dense bone in the centre cavity.

The whole procedure was repeated three times separated over time on the same accelerator giving three measurement points for every position and material. For these measurements, the aggregated mean value of the individual mean HU values was calculated as well as the related SD. The study also evaluated HUs in the FOV for one Siemens CT system. This was based on one measurement.

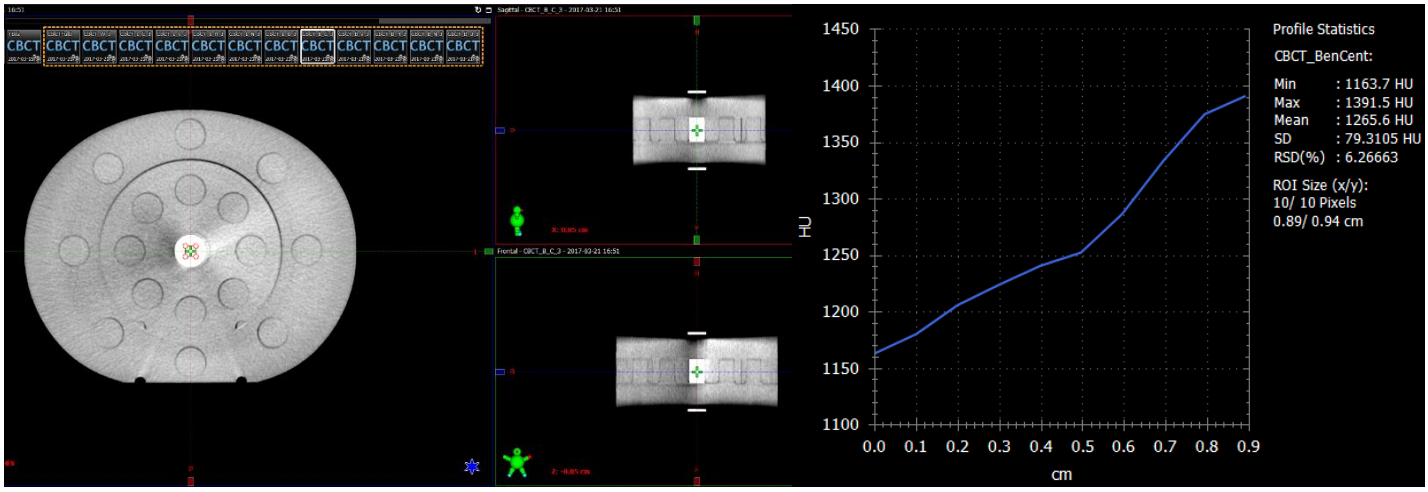

Figure 4. The ROI used to extract HU in various positions for lung inhale, water and solid dense bone 1250 mg/cc HA. The ROI was applied in the centre of each position. In this image, the ROI is applied on solid dense bone 1250 mg/cc HA placed in the centre position.

3.2. Patient specific measurements

3.2.1. Patient material

In this study patients were selected retrospectively from the previously conducted MR-OPERA study, approved by the Ethical Review Board. The patients in the study had undergone radiotherapy either for prostate cancer or for prostate and glandular cancer. For the purpose of the present study, patients treated for both prostate and glandular cancer were selected. These patients had CBCT images acquired as a part of their daily imaging procedure to assure correct patient positioning prior treatment. The CBCT images can be acquired with different parameter settings, depending on the used protocol. For consistency, only CBCT data acquired with the same parameter settings were used and in total data from seven patients were included in the study.

Four CBCT images from each patient were used for the image analysis, giving a total number of 28 CBCT images. All of the CBCT images were acquired in CBCT Pelvis Mode with the predetermined acquisition parameters seen in Table 3. Reconstruction thickness was set to 3 mm, which was the same slice thickness as in the acquired CT images for the patients.

Table 3. The predetermined acquisition parameters for CBCT Pelvis Mode.

Acquisition Parameters	
Fan Type	Half
Trajectory	Full
kV	125
mAs	1080
CTDIw	1.60Gy

3.2.2. HU to RED table

Performing dose calculation requires RED. To obtain this a HU to RED table is used in the TPS transforming HU in CT images to corresponding RED. The table used in the clinic can be seen in Table 6.

It is established that the HUs in CBCT images can differ from the ones in CT images [19][23]. This could mean that the standard HU to RED table (HU-RED CT) used when dose calculating may assign incorrect RED to the CBCT image leading to incorrect dose calculation. To correct this, a different HU to RED table grounded on CBCT images HUs can be used (HU-RED CBCT).

The generation of the HU-RED CBCT table was done in an in-house developed MATLAB (MATLAB R2016a, The MathWorks, Inc., Natick, Massachusetts, United States) program. The generation of the table was population specific which is the preferred method of use according to previous studies [17][24][25]. From each patient, four CBCT data sets were selected and the voxel values were summed up creating a mean value histogram for all patients. For air, fat and muscle the mean HU was extracted from the histogram using peak analysis that generates the locations of local maxima. These values were assigned to the expected corresponding RED described in Table 2. To cover the entire clinically relevant HU span, a value for solid dense bone was desirable. Unfortunately, this could not be obtained using the same method as for air, fat and muscle. To obtain the value, the measurements carried out on the phantom to evaluate the constancy of HU in the FOV was used. The mean HU of solid dense bone was assigned the corresponding RED given in Table 2. A fifth HU value representing materials such as metal had been assigned in the standard HU-RED CT table. This value was matched and corresponding RED was extrapolated assuming a linear relationship.

3.2.3. Treatment Planning

Four out of the seven patients were suitable for treatment planning since the three remaining patients had an insufficient coverage of the target area on the CBCT images, making absorbed dose calculations unfeasible.

For each patient, a sCT data set was created via the MriPlanner™ software (Spectronic Medical AB, Sweden). The sCT images had the same resolution, frame of reference, body outline and FOV as the MRI images. The clinical target volume (CTV), consisted the prostate, and OARs were automatically segmented on the MRI images in the MriPlanner™ software and transferred onto the sCT images. Since the MRI images is the primary image modality in an MRI only workflow, the CT and CBCT images were rigidly registered based on bone anatomy to the sCT and re-sliced to the same slice thickness (2.5 mm) as the MRI images. The body outlines were cropped to be the same as the MRI images. If the body outlines in the CT and CBCT images transcended the body outline in the MRI images, the transcended part was eliminated in the CT and CBCT images. If the situation was reversed the body outlines in the CT and CBCT images was extended with water equivalent HUs resulting in the same body outline as in the MRI

images. The sCT, CT and CBCT images were returned to the Eclipse treatment planning system (Varian Medical Systems, Palo Alto, CA) in the same frame of reference as the MRI images. Re-slicing, body cropping and setting the frame of reference was made as a pre-processing by Spectronic Medical before the images was returned to the TPS.

In this study RapidArc was the technique chosen to generate an initial treatment plan on the sCT images. The PTV was created by 7 mm expansion of the CTV in all directions. The energy used was 10 MV and the prescribed dose was 78 Gy with 2 Gy per fraction, concluding in a total of 39 fractions. In Eclipse TPS, the Dose Volume Optimizer (v. 10.0.28) was used for plan optimisation and final dose calculation was performed with the AAA (Anisotropic Analytical Algorithm v. 13.6.23). The sCT plan was normalised to 100% to the mean PTV target dose. All treatment plans were set to fulfil the dose volume constraints for the conventional arm in the Swedish multicentre Phase III study of HYPO-fractionated Radiotherapy of intermediate risk localised Prostate Cancer (HYPO-RT-PC) [28]. The constraints can be seen in Table 4.

To enable evaluation in between absorbed dose calculations carried out on sCT, CT and CBCT images, the structure set from the sCT images was copied and transferred to the CT and CBCT images. The treatment plan copied to the CT and CBCT images was creating plans identical to the initial sCT plan. For the CBCT images, the treatment plan was recalculated twice, first with the original HU-RED CT table applied on the CBCT images and then with the developed HU-RED CBCT table, both seen in Table 6. This concluded in four different plans for each patient denoted sCT, CT, $CBCT_{HU\text{-}RED\ CT}$, $CBCT_{HU\text{-}RED\ CBCT}$.

Table 4. The dose volume constrains for the conventional arm in the HYPO-RT-PC study. The priority of fulfilling the dose volume constrain can be seen as well as what volume the dose volume constrain influence.

Priority	Volume	Dose Volume Constraints
1	CTV	$D_{min} \geq 95\%$ $D_{min} \geq 74$ Gy
2	PTV	$V_{95\%} \geq 95\%$ $V_{74Gy} \geq 95\%$
3	Rectum	$V_{90\%} \leq 15\%$ $V_{70Gy} \leq 15\%$
4	PTV	$D_{99\%} \geq 90\%$ $D_{99\%} \geq 70$ Gy
5	Rectum	$V_{75\%} \leq 35\%$ $V_{59Gy} \leq 35\%$
6	Femoral heads	$D_{max} \leq 70\%$ $D_{max} \leq 55$ Gy
7	Rectum	$V_{65\%} \leq 45\%$ $V_{51Gy} \leq 45\%$
8	Body	$D_{max} \leq 105\%$

3.2.4. Evaluation

To evaluate the differences in the four dose distributions MICE (Medical Interactive Creative Environment, v. 0.4.0.0, available at www.gentleradiotherapy.se) was used. This is a program that, by using the total plan dose matrix and structure set, can produce dose volume histograms and extract data that is of interest. Data of interest were the dose volume constraints from the HYPO-RT-PC study and the mean absorbed dose to the PTV, CTV and OARs.

The difference in absorbed dose between the plans was then compared as CT/sCT, $CBCT_{HU\text{-}RED\ CT}$/sCT and $CBCT_{HU\text{-}RED\ CBCT}$/sCT for each patient. The mean value and SD for all patients was

calculated. For one of the patients, the CBCT image did not cover the entire rectum and therefore the rectum related dose volume constraints and rectum mean absorbed dose were excluded.

4. Results

4.1. Phantom measurements

4.1.1. Constancy of HU over time

Figure 5 displays the aggregated mean HU value calculated from the measurements investigating the constancy of HU over time. HUs and corresponding SD for each tissue equivalent electron density plug are illustrated.

The SD for the materials, excluding solid dense bone, ranged from 5.86 - 17.5 HU. Solid dense bone inserts, both with 800 and 1250 mg/cc, had a slightly larger SD at 27.9 and 39.6 respectively compared to the other tissue inserts. Relative standard deviation was 3.21% for solid dense bone 800 mg/cc and 2.82% for solid dense bone 1250 mg/cc. The corresponding values for lung exhale and muscle was 0.91% and 11.4% respectively.

All the HU values were within reasonable expected values acknowledged in Table 1. The maximum difference measured was for lung exhale inner and outer. These values were 153 HU and 105 HU higher that the highest value in the span.

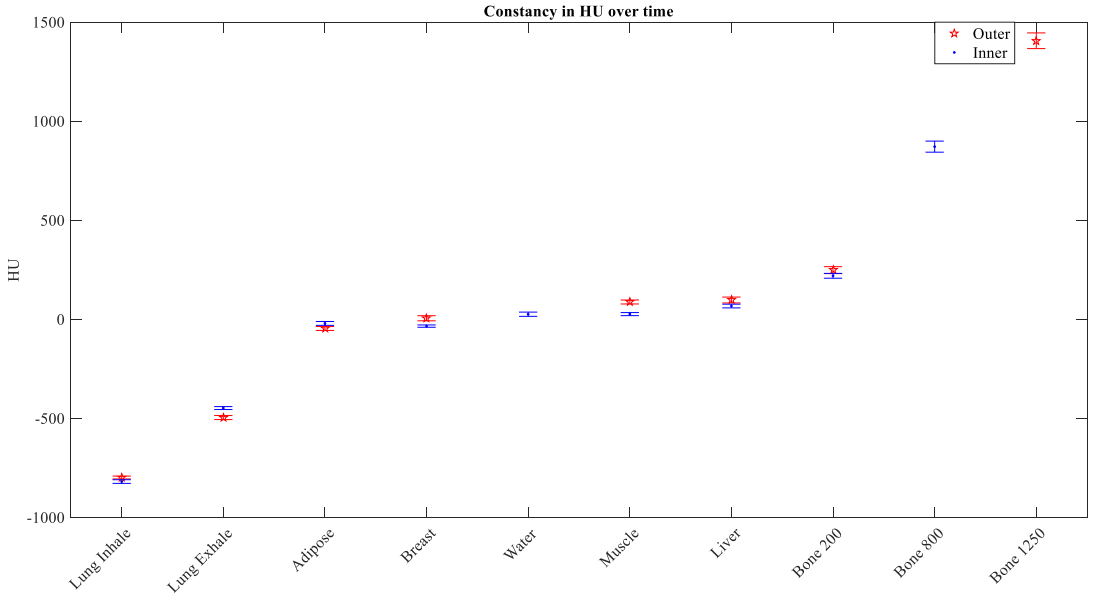

Figure 5. The mean HU value for ten tissue equivalent electron density plugs. Values denoted with a pentagram represented the plugs located in the outer disk. Values denoted with a dot represented the plugs located in the inner disk.

4.1.2. Consistency of HU between kV CBCT systems

The aggregated mean value of the individual mean HU values measured on the six kV CBCT system available in the clinic is illustrated in Figure 6. HUs and corresponding SD for each material inserts are shown.

The largest difference between the accelerators was found for solid dense bone 1250 mg/cc. This was 178 HU and was considered small. The SD for all the materials, except solid dense bone 1250 mg/cc, ranged from 10.2 - 49.7 HU from the mean values. The SD for solid dense bone 1250 mg/cc was slightly larger (68.6 HU). The location of the material in the inner or outer disk did not affect the HU. In general, all the HUs for every material overlapped within one SD.

The HU for all the materials had values that were reasonable compared to the one acknowledged in Table 1.

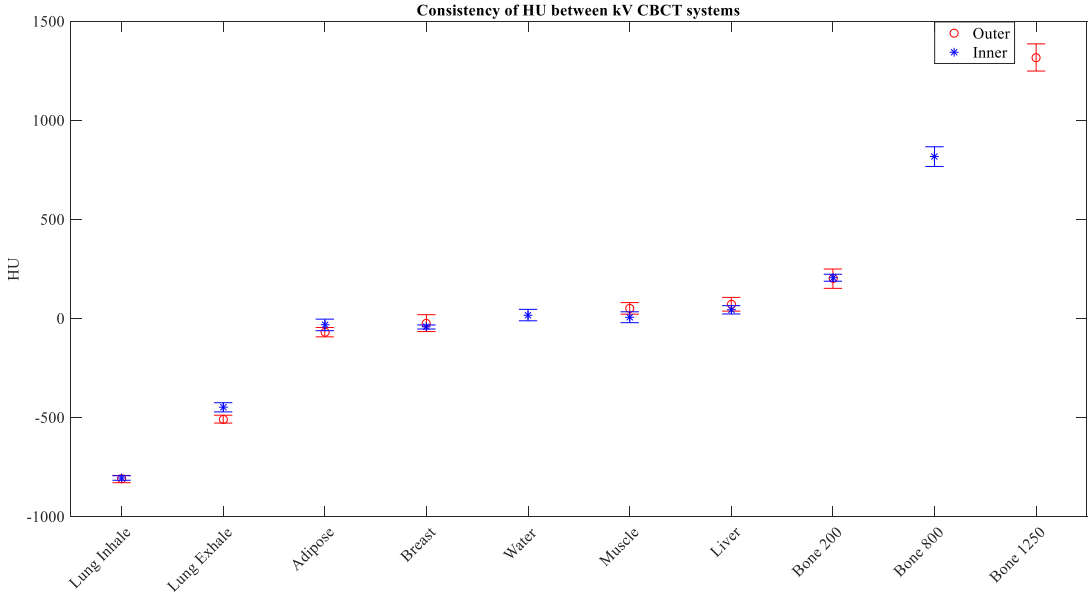

Figure 6. The mean HU value for the different materials measured on six kV CBCT systems. Value denoted with a circle represented the electron density plugs located in the outer disk. Values denoted with a star represented the electron density plugs located in the inner disk.

4.1.3. Constancy of HU in FOV

The aggregated mean HU value and SD in the FOV were demonstrated in Table 5, for CBCT and CT images. The deviation in HU between CT and CBCT images was minor. The largest difference in aggregated mean HU was 59 HU and seen for the solid dense bone 1250 mg/cc HA insert. Lung inhale and water inserts had a difference in aggregated mean HU of 30 HU. The relative standard deviation in lung inhale, water and solid dense bone 1250 mg/cc was for CT image 0.03%, 2.77% and 1.04% and for CBCT image 2.85%, 82.4% and 8.56% respectively.

HU could be shown to fluctuate more within the CBCT images then in the CT images. The SD for lung inhale and solid dense bone within the CBCT images were approximately nine times larger than for the CT image. For water the SD was four times larger than in the CT image.

Table 5. Aggregated mean HU values and SD for the different materials based on one CT and three CBCT data sets. The materials evaluated was lung inhale, water and solid dense bone 1250 mg/cc HA.

	HU Lung Inhale		**HU Water**		**HU Solid dense bone**	
Image	Mean	SD	Mean	SD	Mean	SD
CT	-779	2.45	-1.94	5.37	1237	12.9
CBCT	-808	23.0	28.4	23.4	1296	111

4.2. Patient specific measurements

4.2.1. HU to RED table

The patient used to develop the HU-RED CBCT table had median weight of 87 kg and was 76 years old. In Table 6a, the standard HU-RED CT table were showed. In Table 6b, the generated

HU-RED CBCT table. The first three HU value points represented air, fat and muscle were based on 28 CBCT images. The fourth was the mean value of solid dense bone measured in phantom. The fifth HU value point was selected to match the HU-RED CT and the corresponding RED was extrapolated assuming a linear relationship.

Table 6a and 6b. The two HU-RED tabled used for absorbed dose calculation. The standard HU-RED CT (a) and the generated HU-RED CBCT (b).

HU-RED CT	
HU Value [HU]	RED
-1000	0,000
-100	0,900
100,0	1,100
1000	1,532
6000	3,920

a)

HU-RED CBCT	
HU Value [HU]	RED
-1000	0,000
-102,0	0,949
26,00	1,043
1296	1,695
6000	4,110

b)

4.2.2. Treatment planning

The four plans created for every patient fulfilled the dose volume constrains except two plans for one patient. This was the CT plan and $CBCT_{HU\text{-}RED\ CT}$ plan. For these plans, maximum global dose (Body D_{max}) exceeded 105% of the prescribed dose by 0.5%, which was minor and therefore did not have any impact on the result.

The mean difference in absorbed dose for specific DVH metrics comparing the dose distributions for CT, $CBCT_{HU\text{-}RED\ CT}$ and $CBCT_{HU\text{-}RED\ CBCT}$ to the sCT dose distribution can be seen in Figure 7. The baseline of zero represents no difference between the DVH metrics compared. A deviation from the baseline represents a difference. The complete data for each patient can be seen in Appendix 1.

The result for the comparison between sCT and CT dose distribution shows a small deviation for all DVH metrics evaluated. The maximum deviation is 0.2% corresponding to the rectum $V_{90\%}$ point. The SD ranges from 0.0% to 0.5%.

The difference in DVH metrics for the $CBCT_{HU\text{-}RED\ CT}$/sCT dose distribution comparison is smaller for the PTV and CTV DVH metrics and in general larger for the OARs DVH metrics compared to CT/sCT dose distribution. All the DVH metrics, excluding the body max point, have a deviation that was lower than 0.3%. The SD is in general the same as the CT/sCT dose distribution comparison for all DVH metrics. The SD ranges from 0.1% to 0.5%.

The $CBCT_{HU\text{-}RED\ CBCT}$/sCT dose distribution comparison shows a deviation that is larger for most of the DVH metrics compared to the other comparisons. The largest deviation noted can be seen for PTV and CTV DVH metrics, but the deviations are below 1%. In this comparison, the SD is between 0.0% and 0.4%

The results conclude that all the comparisons have a high agreement with all the DVH metrics with a similar set of standard deviations.

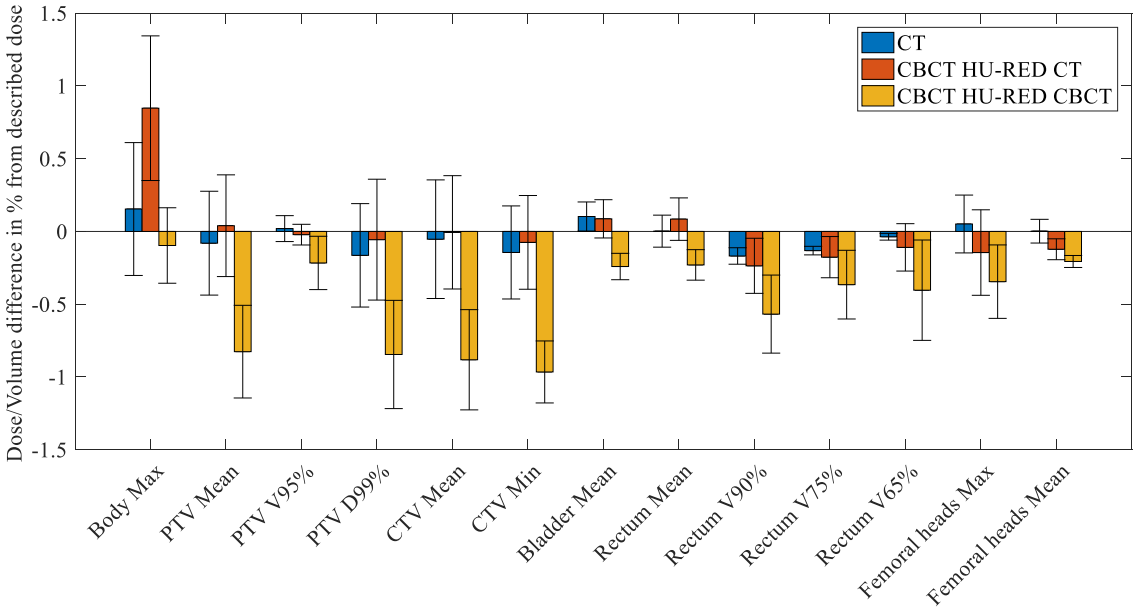

Figure 7. Percentage mean absorbed dose difference for specified DVH metrics for the three comparisons, CT/sCT (blue), $CBCT_{HU\text{-}RED\ CT}$ /sCT (red) and $CBCT_{HU\text{-}RED\ CBCT}$ /sCT (yellow).

5. Discussion

5.1. Phantom measurements

If the verification of sCT images is founded on CBCT images, it is essential to know how the kV CBCT systems behaves. Various measurements have therefore been carried out investigating different aspects. These measurements were carried out on a phantom in order to maintain a repeatable process.

The results from the phantom measurements showed that the HUs were constant over 9 weeks period for all materials. This indicated that the system was robust and did not drift, allowing accurate HU measurements over time. No significant difference in HU was observed between the six kV CBCT systems in the clinic. This showed that all the CBCT systems generated HUs that were comparable to each other within the same material. Results from one kV CBCT system could be applied on all the systems. This is similar to previous results reported for Varian On-Board Imager TrueBeam [25]. The CBCT images exhibited similar mean HU values as the CT images which was also in agreement with previous work [25]. This indicated that a correction of the HUs was not needed for CBCT images. The SD was higher within the FOV for CBCT HU values then for CT HU values. This suggests that the CIRS Model 062M Electron Density Phantom may not be optimal for CBCT measurements and that a dedicated phantom for CBCT measurements might be a more suitable choice. This because a dedicated phantom for CBCT is designed to provide a reliable tool for HU to RED calibration in volumetric imaging using additional scattering material.

The result presented in Figure 5 showed the constancy of HU over time for inserts with different tissue equivalent densities for one kV CBCT system. Comparing the measured values with the ones denoted in Table 1 a maximum difference of 153 HU and 105 HU for lung exhale inner and outer could be seen. The air value in Table 1 does not give any information about how it has been estimated and may not be measured in the same stage as lung exhale. This could be an explanation why this tissue exhibits the larges deviation. The SD for all of the electron density plugs was small compared to the uncertainty in HU accuracy estimated by IAEA in the publication about accuracy requirements and uncertainties in radiotherapy [29]. For a kV CBCT image the HU accuracy was estimated to be between 20-100 HU. Since the largest deviation was 39.6 HU it could be concluded that the HUs is constant over time for all materials for a Varian On-Board Imager TrueBeam.

Skåne University Hospital has six different Varian On-Board Imager TrueBeam. Figure 6Figure 6 displayed the mean HU value and SD for all kV CBCT systems, for each tissue equivalent electron density plug. When a CBCT system was installed a HU acceptance test was carried out. A tolerance level of $\pm$50 HUs from the expected HU value must be achieved for materials ranging from -1000 HU to 120 HU. The SD from the mean HU value for all kV CBCT systems for materials within -1000 HU to 120 HU, had a value that were lower than the tolerance level. The acceptance test did not contain a tolerance level for high density material, but looking at the material that exceeded 120 HU, i.e. bone, two out of three points had a SD that was below 50 HU. Solid dense bone 1250 mg/cc had a SD that was 68.6 HU but since the HU accuracy for a kV CBCT image was estimated to be 20-100 HU [29], a surplus of 18.6 HU is insignificant. The results presented indicate that all the CBCT systems generate HUs that are comparable to each other for the investigated materials.

Studying the result in Table 5, it can be seen that the difference in mean HU between CBCT images and CT images is minor. The difference for lung inhale and water is approximately 30 HU. For solid dense bone, a difference of 59 HU is established. Compared to the expected HU accuracy for a kV CBCT system [29] the differences are negligible. This suggests that a correction of the HU may not be necessary. The SD was higher for the mean HU estimated in the CBCT images compared to the SD for the mean HU estimated in the CT image. The mean HU in the CBCT images had a SD that was four to nine times larger, depending on which material, compared to the SD for the mean HU in the CT image. It has been shown in previous work [30] and stated in the theory [23]

that a large scan object entails larger presence of scatter for the cone beam geometry. The increase in scatter contamination affected the reconstruction of the image resulting in an impact on the HUs. This might be one explanation of why there was higher SD within the FOV of the CBCT images. The measurements carried out in this thesis were done using a phantom, with a size representing an abdomen configuration. This size is classified as a larger object which leads to an increase in the scatter contamination for the CBCT images compared to the CT images.

5.2. Patient specific measurements

In external radiotherapy, it is essential to ensure that high accuracy is maintained. To be able to do that quality controls and quality assurance is carried out throughout the radiotherapy chain. When introducing treatment planning on sCT images it must be ensured that the images have been generated correctly and that they provide the same information as the CT images would have. In an MRI only workflow, creating treatment plans with the CBCT as the image material and then comparing the dose distribution with the sCT based treatment plan is a method we propose to ensure quality accuracy of the sCT image.

Edmund *et al.* has in previous work presented a way to verify the sCT data using the CBCT data. By creating HU-RED curves and statistically analysing median value of the binned absolute errors, they concluded that verification of the sCT data could be done with CBCT data using a population based calibration curve [17]. From this study, interest arose in further work to calculate absorbed dose on CBCT images with a population based HU-RED table to verify the sCT images which was not investigated in Edmund *et al.*

Previous work had also established that it was possible to accurately calculate absorbed dose on CBCT images. To obtain an accurate calculation, Richer *et al.* used a population based HU-RED table to correct HUs. This method gave a difference in absorbed dose, between calculations carried out on CT and CBCT images, that was less than 5% comparing DVH metrics [24]. de Smet *et al.* used the same approach to obtain accurate absorbed dose calculation. Their study showed that there was no need for HU correction when using kV CBCT systems from Varian TrueBeam. Using the standard HU-RED CT gave differences of 2% to 3 % for pelvis patients comparing DVH metrics. A population based HU-RED CBCT gave a better agreement. The difference was then 1% to 2% comparing DVH metrics [25]. In this study, a population based HU-RED CBCT table with one phantom based HU value was used for absorbed dose calculation. This was because previous work [17][24][25] has concluded that a population based table provides an accurate enough HU to RED conversion for CBCT images. It would have been preferable to use the same method to decide on the appropriate HU value for solid dense bone; however the lack of intensity of solid dense bone voxels prevented the HU value being extracted in this way. Thresholding is another method that amplifies the intensity for solid dense bone voxels, and this method could potentially give a more accurate result. This has, however, not been part of this study.

Studying Figure 7, the mean difference in absorbed dose between CT, CBCT and sCT plans is small. The maximum difference is less than 1% which can be considered negligible compared to the desired and achievable levels of overall dose accuracy. Published data has suggested an acceptable level of overall dose accuracy to be between 3.5% and 5% [29]. All the invested treatment plans generated dose distributions with differences in mean dose well within the clinical tolerance. This concludes that recalculating treatment plans on the CBCT image and comparing the dose distribution to the calculation carried out on the sCT image can detect gross errors in the sCT image, regardless of density table used. Hence, the CBCT image can be used to ensure quality accuracy of the sCT image.

Dose distributions on the CBCT image with HU-RED CBCT generally resulted in the largest mean dose differences for all the investigated DVH metrics. The choice of density table is the only thing separating the treatment plans done on the CBCT images. This indicates that the standard HU to density table provides a more accurate HU to RED transformation than the CBCT based HU to density curve. The HU-RED CBCT should provide a more accurate dose distribution since the FOV varies more within CBCT images than CT images. Why this is not the case may be that the method of developing the HU-RED CBCT is not optimal. The extraction of the solid dense bone HU may affect the outcome result. Although since the amount of solid dense bone that is present in the investigated anatomy are expected to be fairly small. Therefore, this is likely to have a small impact on the dose calculation. A suggestion of improvement would be to use of deformable image registration to extract bone values and avoid the use of histograms, which were insufficient in this aspect.

The structure set from the sCT images was copied and transferred onto the CT and CBCT images. All the datasets structures will then have the same volume size and position enabling the same treatment plan to be used. This contributes to a more impartial dose comparison. Although copying the structure set may contribute to mismatches with the CT and/or CBCT images. The delineated organs on the MRI images should not differ from the CT and/or CBCT images but due to variety in patient set up and/or dissimilar intestinal filling between the image sessions, this could be the case. If this is the case, the comparison of the mean dose difference may be affected. Deformable image registration could have been used to eliminate this affect. But the use of deformable image registration in a clinical setup may not be preferable.

This study showed that verification of the sCT image can be done via dose distribution comparison between calculations carried out with sCT and CBCT images as basis. Recalculating the plan on the CBCT image resulted in a difference of mean dose to the PTV of 0.0% (HU-RED CT) and -0.8% (HU-RED CBCT) when comparing calculations based on sCT and CBCT images. These uncertainties appear to be negligible compared to the overall dose accuracy.

6. Conclusion

Phantom measurements showed that the kV CBCT systems at the clinic were stable in HU over time and relative to each other. The variation in HUs between one CBCT system and one CT system was considered to not have clinical impact. Differences between patient specific absorbed dose calculations based on sCT and CBCT images were small and considered to be within clinical tolerance. This indicates that dose plan recalculating on CBCT images for sCT images verification can be used in an MRI only workflow.

7. Future perspective

In this study, the method of creating the HU-RED CBCT table was not optimal. The value for solid dense bone was obtained by using a phantom based measurement instead of patient based. Further work investigating other methods to estimate HUs based on patients would be interesting. Methods to filter out solid dense bone HU values in the CBCT image was tested as part of this project, but without success. Development of the filter method could be done or another approach could be tested. Applying threshold on the CBCT images may result in a patient based solid dense bone HU value.

The aim in verifying the sCT image is mainly to detect catastrophic errors. The work done in this thesis contained comparisons with successfully generated sCT data sets. It would be of interest to investigate if the method could detect catastrophic errors in the sCT image. This is something that may be necessary to evaluate before actually using the CBCT image to verify the sCT image in a clinical workflow.

Some patients lose weight during their treatment, changing their body contour and therefore altering the dose distribution. For these cases, it is of interest to evaluate whether the absorbed dose still fulfills the constrains for the PTV and OARs. One approach to investigate this is to recalculate the absorbed dose on a CBCT image. Treatment planning on Varian TrueBeam CBCT images showed that this could be done with the standard HU-RED CT table since it creates accurate dose distributions.

This thesis focused on patient with prostate glandular cancer. It would be of interest to investigate whether the method of verifying the sCT image could be applied in other regions.

8. References

[1] "Cancerfondsrapporten 2016," 2016.

[2] "Strålbehandling | Cancerfonden." [Online]. Available: https://www.cancerfonden.se/om-cancer/stralbehandling?gclid=CjwKEAiArbrFBRDL4Oiz97GP2nISJAAmJMFaQchzIlyUZDml8YaQR874dpu-W_IrJ4aIOW-OhvXU2xoCPJfw_wcB. [Accessed: 23-Feb-2017].

[3] B. Hentschel, W. Oehler, D. Strauß, A. Ulrich, and A. Malich, "Definition of the CTV Prostate in CT and MRI by Using CT–MRI Image Fusion in IMRT Planning for Prostate Cancer Strahlentherapie und Onkologie," *Strahlenther Onkol*, no. 3, 2011.

[4] P. L. Roberson, P. W. McLaughlin, V. Narayana, S. Troyer, G. V. Hixson, and M. L. Kessler, "Use and uncertainties of mutual information for computed tomography/magnetic resonance (CT/MR) registration post permanent implant of the prostate," *Med. Phys.*, vol. 32, no. 2, pp. 473–482, Jan. 2005.

[5] M. E. Korsholm, L. W. Waring, and J. M. Edmund, "A criterion for the reliable use of MRI-only radiotherapy.," *Radiat. Oncol.*, vol. 9, p. 16, Jan. 2014.

[6] C. Rasch, I. Barillot, P. Remeijer, A. Touw, M. van Herk, and J. V Lebesque, "Definition of the prostate in CT and MRI: a multi-observer study," *Int. J. Radiat. Oncol.*, vol. 43, no. 1, pp. 57–66, 1999.

[7] M. Roach, P. Faillace-Akazawa, C. Malfatti, J. Holland, and H. Hricak, "Prostate volumes defined by magnetic resonance imaging and computerized tomographic scans for three-dimensional conformal radiotherapy," *Int. J. Radiat. Oncol.*, vol. 35, no. 5, pp. 1011–1018, Jul. 1996.

[8] J. A. Dowling *et al.*, "An Atlas-Based Electron Density Mapping Method for Magnetic Resonance Imaging (MRI)-Alone Treatment Planning and Adaptive MRI-Based Prostate Radiation Therapy," *Int. J. Radiat. Oncol.*, vol. 83, no. 1, pp. e5–e11, 2012.

[9] J. M. Edmund, H. M. Kjer, K. Van Leemput, R. H. Hansen, J. AL Andersen, and D. Andreasen, "A voxel-based investigation for MRI-only radiotherapy of the brain using ultra short echo times," *Phys. Med. Biol.*, vol. 59, no. 23, pp. 7501–7519, Dec. 2014.

[10] A. Johansson, M. Karlsson, J. Yu, T. Asklund, and T. Nyholm, "Voxel-wise uncertainty in CT substitute derived from MRI," *Med. Phys.*, vol. 39, no. 6, pp. 3283–3290, 2012.

[11] J. Lambert *et al.*, "MRI-guided prostate radiation therapy planning: Investigation of dosimetric accuracy of MRI-based dose planning," *Radiother. Oncol.*, vol. 98, no. 3, pp. 330–334, 2011.

[12] S.-H. Hsu, Y. Cao, K. Huang, M. Feng, and J. M. Balter, "Investigation of a method for generating synthetic CT models from MRI scans of the head and neck for radiation therapy," *Phys. Med. Biol.*, vol. 58, no. 23, pp. 8419–8435, Dec. 2013.

[13] J. Korhonen, M. Kapanen, J. Keyriläinen, T. Seppälä, and M. Tenhunen, "A dual model HU conversion from MRI intensity values within and outside of bone segment for MRI-based radiotherapy treatment planning of prostate cancer," *Med. Phys.*, vol. 41, no. 1, p. 11704, Dec. 2013.

[14] D. Andreasen, K. Van Leemput, R. H. Hansen, J. A. L. Andersen, and J. M. Edmund, "Patch-based generation of a pseudo CT from conventional MRI sequences for MRI-only radiotherapy of the brain," *Med. Phys.*, vol. 42, no. 4, pp. 1596–1605, 2015.

[15] M. Köhler, T. Vaara, M. Van Grootel, R. Hoogeveen, R. Kemppainen, and S. Renisch, "MR-only simulation for radiotherapy planning treatment planning," *White Pap. Philips MRCAT prostate dose Calc. using only MRI data*, pp. 1–16, 2015.

[16] C. Siversson *et al.*, "Technical Note: MRI only prostate radiotherapy planning using the statistical decomposition algorithm," *Med. Phys.*, vol. 42, no. 10, pp. 6090–6097, 2015.

[17] J. M. Edmund, D. Andreasen, F. Mahmood, and K. Van Leemput, "Cone beam computed tomography guided treatment delivery and planning verification for magnetic resonance imaging only radiotherapy of the brain," *Acta Oncol. (Madr).*, vol. 54, no. 9, pp. 1496–1500, 2015.

[18] I. M. D. Dance, S. Christofides, M. Maidment, "Diagnostic Radiology Physics: A handbook for teachers and students," *Iaea*, p. 710, 2014.

[19] "Radiological Protection in Cone Beam Computed Tomography (CBCT)," *ICRP Publ. 129*, vol. 2, no. 1, pp. 1–4, 2015.

[20] N. Wen *et al.*, "Dose delivered from Varian's CBCT to patients receiving IMRT for prostate cancer," *Phys. Med. Biol.*, vol. 52, no. 8, pp. 2267–2276, Apr. 2007.

[21] E. Persson *et al.*, "MR-OPERA: A Multicenter/Multivendor Validation of Magnetic Resonance Imaging–Only Prostate Treatment Planning Using Synthetic Computed Tomography Images," *Int. J. Radiat. Oncol.*, Jun. 2017.

[22] D. Tack, M. Kalra, and P. Gevenois, *Radiation Dose from Multidetector CT*. 2012.

[23] J. H. Siewerdsen and D. A. Jaffray, "Cone-beam computed tomography with a flat-panel imager: Magnitude and effects of x-ray scatter," *Med. Phys.*, vol. 28, no. 2, pp. 220–231, Feb. 2001.

[24] A. Richter *et al.*, "Investigation of the usability of conebeam CT data sets for dose calculation," *Radiat. Oncol.*, vol. 3, no. 1, p. 42, 2008.

[25] M. de Smet, D. Schuring, S. Nijsten, and F. Verhaegen, "Accuracy of dose calculations on kV cone beam CT images of lung cancer patients," *Med. Phys.*, vol. 43, no. 11, pp. 5934–5941, 2016.

[26] A. Dunlop *et al.*, "Comparison of CT number calibration techniques for CBCT-based dose calculation.," *Strahlenther. Onkol.*, vol. 191, no. 12, pp. 970–978, 2015.

[27] CIRS, "CBCT Electron Density & Image Quality Phantom System. Model 062M, Model 062MA, Model 062MQA. USER GUIDE."

[28] A. Widmark, "Phase III study of HYPOfractionated RadioTherapy of intermediate risk localised Prostate Cancer," *doi.org*.

[29] "IAEA HUMAN HEALTH SERIES No. 31 Accuracy Requirements and Uncertainties in Radiotherapy," no. 31, 2016.

[30] Y. Rong, J. Smilowitz, D. Tewatia, W. A. Tomé, and B. Paliwal, "Dose Calculation on KV Cone Beam CT Images: An Investigation of the Hu-Density Conversion Stability and Dose Accuracy Using the Site-Specific Calibration," *Med. Dosim.*, vol. 35, no. 3, pp. 195–207, 2010.

Appendix 1

RapidArc treatment planning. The DVH comparison between CT/sCT, $CBCT_{HU\text{-}RED\ CT}$/sCT and $CBCT_{HU\text{-}RED\ CBCT}$/sCT for each patient is shown in the table.

	Patient 1			Patient 2		
	CT	$CBCT_{HU\text{-}RED\ CT}$	$CBCT_{HU\text{-}RED\ CBCT}$	CT	$CBCT_{HU\text{-}RED\ CT}$	$CBCT_{HU\text{-}RED\ CBCT}$
Body Max	0.1	1.0	-0.1	-0.4	0.2	-0,5
PTV Mean	-0.4	-0.2	-1.1	-0.4	-0.3	-1,1
PTV V95%	-0.1	-0.1	-0.4	-0.0	-0.0	-0,1
PTV D99%	-0.5	-0.5	-1.2	-0.3	-0.2	-1,1
CTV Mean	-0.4	-0.3	-1.2	-0.4	-0.3	-1,2
CTV Min	-0.4	-0.2	-1.1	-0.5	-0.4	-1,2
Bladder Mean	0.1	0.0	-0.2	-0.0	-0.0	-0,3
Rectum Mean	-0.1	-0.0	-0.3	-0.0	0.0	-0,2
Rectum V90%	-0.1	-0.1	-0.5	-0.2	-0.1	-0,4
Rectum V75%	-0.1	-0.1	-0.3	-0.1	-0.1	-0,2
Rectum V65%	-0.1	-0.1	-0.3	-0.0	0.0	-0,1
Femoral Heads Max	-0.1	-0.2	-0.3	-0.2	-0.5	-0,7
Femoral Heads Mean	-0.0	-0.2	-0.2	-0.1	-0.2	-0,3

Appendix 1 – continue

	Patient 3			Patient 4		
	CT	$CBCT_{HU-RED\ CT}$	$CBCT_{HU-RED\ CBCT}$	CT	$CBCT_{HU-RED\ CT}$	$CBCT_{HU-RED\ CBCT}$
Body Max	0.3	1.4	0.2	0.7	0.7	-0.0
PTV Mean	0.2	0.4	-0.5	0.3	0.2	-0.6
PTV V95%	0.0	0.0	0.0	0.1	0.0	-0.4
PTV D99%	-0.3	0.4	-0.6	0.4	0.1	-0.5
CTV Mean	0.3	0.4	-0.5	0.3	0.2	-0.6
CTV Min	0.2	0.4	-0.7	0.1	-0.1	-0.9
Bladder Mean	0.1	0.0	-0.3	0.2	0.3	-0.1
Rectum Mean	0.1	N/A	N/A	0.1	0.3	-0.1
Rectum V90%	-0.2	N/A	N/A	-0.2	-0.5	-0.9
Rectum V75%	0.0	N/A	N/A	-0.2	-0.3	-0.6
Rectum V65%	0.3	N/A	N/A	-0.0	-0.3	-0.8
Femoral Heads Max	0.2	0.1	-0.1	0.3	0.0	-0.2
Femoral Heads Mean	0.0	-0.1	-0.2	0.1	-0.0	-0.2